Integration of Torque Controlled Arm with Velocity Controlled Base for Mobile Manipulation: An Application to Aircraft Canopy Polishing

Denny Oetomo[1], Marcelo Ang Jr.[1], Rodrigo Jamisola[2], Oussama Khatib[3]

[1] Department of Mechanical Engineering, National University of Singapore, Singapore
[2] Department of Electrical Engineering, Colorado State University, USA
[3] Computer Science Department, Stanford University, USA.

Abstract. A mobile manipulation system often involves combining more than one robot together, typically a manipulator arm and a mobile base. To implement a force and motion control with dynamic compensation, a torque-controlled system is necessary. However, a torque-controlled robot is not always available. In fact, most commercially available mobile bases are velocity-controlled. This paper presents a method for combining a torque-controlled arm and a velocity-controlled base, while performing a force and motion task. The operational space formulation using a consistent set of integrated arm-base robot dynamics is employed in a mobile manipulation task of polishing an aircraft canopy. The torque controlled arm compensates for the dynamics introduced by the mobile base. The added mobility of the base enables the arm to cover the entire workspace.

1 Introduction

In mobile manipulation [Khatib et al. (1999)], a manipulator arm is typically mounted on a mobile base, and the arm and base are in simultaneous motion during a manipulation task. The capabilities of the arm to manipulate and interact with the environment is very much extended with the large reachable workspace of the mobile base. When implemented in operational space formulation [Khatib (1987)], ideally, we would like to have the resulting system as one dynamically compensated system. For that to take place, both arm and base need to be in torque control mode. However, most commercially available mobile bases are velocity-controlled. In this paper, we show a solution to the problem by combining the operational space formulation with a kinematic-based control (velocity control) while maintaining dynamic compensation.

The dynamic model of the entire mobile manipulator is first derived. Control algorithms using the complete dynamic model are then formulated. The algorithms compute torque and velocity commands for the torque-controlled and velocity-controlled joints, respectively, to execute the desired end-effector task. The operational space formulation [Khatib (1987)] is utilized to generate the torque command vector, taking into account the complete arm-base dynamics as seen from the operational point. Utilizing the property of the dynamically consistent inverse [Chang and Khatib (1995)], $\bar{J}$ is used not only in producing the torque control command, but also the velocity control commands.

The resulting system is capable of dynamically compensated unified force and motion control. The method is implemented on a PUMA 560 arm and the NOMAD XR4000+ base (Figure 1). The arm provides 6 degrees of freedom for articulation while the base provides 3 degrees

of freedom in the plane and extends the workspace of the manipulator arm to cover the entire canopy. All the six joints of the PUMA arm is torque-controlled. The NOMAD base is independently driven by 8 DC motors that are not capable of velocity control. Furthermore, velocity command at the motor level is not possible and base motion can be only commanded using high level commands for the holomomic motion in the plane. We therefore treat the base as a 3-DOF velocity controlled system.

This paper presents the result of the implementation of the method on the PUMA - Nomad system. The performance of the system in free motion and force control task was studied. The method is then applied to an industrial application involving an aircraft canopy polishing task. The task is similar to earlier experiment by Grabits (1986), although in the former, the surface of the canopy is first mapped, and therefore known to the robot. The application of our method is on a task that requires the mobile manipulator to maintain a constant force perpendicular to the unknown surface of the canopy, while the polishing tool covers the entire surface to be polished.

2 Operational Space Formulation

The Operational Space Formulation [Khatib (1987)] is a control approach where the robot dynamics is expressed in operational space (Cartesian space as seen from the end-effector or tool). The desired motion and contact forces are then incorporated into force commands at the task level. These commands together with the robot dynamics in operational space are then used to compute the required joint torques which are sent directly to the torque-controlled joint motors.

The operational space force is a combination of the force for free motion (position control) and force for constrained motion (force control). It is then converted to joint torques by

$$\begin{array}{c} \mathbf{\Gamma} = J^T \mathbf{F} + \mathcal{N}^T \mathbf{\Gamma}_0 \\ \mathcal{N} = [I - J^\sharp J] \end{array} \tag{1}$$

where $\mathbf{\Gamma}$ is the required joint actuator values, J is the manipulator Jacobian in operational space, and $\mathcal{N}$ is the null space of J. Null space torque $\mathit{\Gamma}_0$ is used to control the null motions. $J^\sharp$ is a generalized inverse. The use of projection onto the null space would produce an effect whereby any internal motion would not affect the end-effector task. However, this is only true *kinematically* for most generalized inverses. In our method, we used the *dynamically consistent generalized inverse*, $\bar{J}$, defined as:

$$\bar{J} = A^{-1} J^T \mathit{\Lambda} \tag{2}$$

where A and $\mathit{\Lambda}$ are the inertia matrix in joint and operational space respectively. This inverse minimizes the kinetic energy of the system and guarantees that any projection onto the null space would have no effect on the end-effector task *dynamically*.

The dynamically compensated operational forces required (**F**) is:

$$\mathbf{F} = \hat{\mathit{\Lambda}}(\mathbf{x})(\mathit{\Omega}\mathbf{F}_{motion} + \bar{\mathit{\Omega}}\mathbf{F}_{force}) + \hat{\boldsymbol{\mu}}(x, \vartheta) + \hat{\mathbf{p}}(x) + \bar{\mathit{\Omega}}\mathbf{F}_{desired} \tag{3}$$

$\mathbf{F}^*_{motion}$ and $\mathbf{F}^*_{force}$ are the operational space forces required to achieve the desired motion and force trajectories. $\mathit{\Omega}$ and $\bar{\mathit{\Omega}}$ are the selection matrices to specify operational space directions that are force and motion controlled. The matrices $\hat{\mathit{\Lambda}}$, $\hat{\mu}$ and $\hat{p}$ are the inertia matrix, Coriolis and Centrifugal matrices, and gravity vector, as seen from the operational space [Khatib (1987)].

3 Velocity Control

As mentioned section 2, the *dynamically consistent inverse* provides the force/position duality, that is exploited in this method to device a velocity control that preserves the dynamic of the structure :

$$\delta \mathbf{q} = \bar{J} d\mathbf{x} + \mathcal{N} \delta \mathbf{q_0} \tag{4}$$

where $\delta \mathbf{q}$ is the command velocity that is the input to the velocity controlled amplifier of the robot. The inverse of Jacobian $\bar{J}$ is the *dynamically consistent inverse* to ensure that the null space dynamics does not interfere with operational space dynamics. The null velocity vector $\delta \mathbf{q}_0$ is utilized to control the posture behavior of the redundant joints, as explained further in Section 4.1.

Typically, velocity controllers operate at a slower rate, (eg. 200Hz), compared to the internal servo (500-1000Hz) at which the torque control is operating. This slower update rate has been known to affect performance.

4 Combined Torque and Velocity Control for Overall System

A mobile manipulator often consists of many joints, and often some are of torque control (typically, the arm) and some of velocity control (typically, the base). In fact, to the best of our knowledge, we are not aware of any commercially available torque-controlled mobile base today. Here we present a method of combining torque and velocity control which is consistent with the dynamics of the entire (eg. arm and base) system. This approach utilizes the force/position duality with extension to the case of redundant manipulators (Eqs. 1 and 4) as shown in Table 1.

Table 1. THE POSITION/FORCE DUALITY

Position	Force
$\delta \mathbf{q} = \bar{J} \delta \mathbf{x} + [I - \bar{J}J] \delta \mathbf{q}_0$	$\Gamma = J^T \mathbf{F} + [I - \bar{J}J]^T \bar{\Gamma}_0$

The approach uses the dynamically consistent inverse, as introduced in Section 2, which guarantees the position/force duality when used in torque control. This property of duality as shown in Table 1, provides a method for us to control the velocity-controlled base in a way which is similar to the RMRC method by Whitney (1969). When used in velocity control, there will be error due to the slower and less accurate macro structure (the base), however, this is compensated by the faster and more accurate mini structure (the arm).

The combined manipulator arm and the mobile base system can now be regarded as an n DOF system, where n is the total number of joints that the two systems have. The Jacobian matrix generated is of size m by n, where m is the number of DOF of the specified task.

Treating the combined system as an n DOF robot, a torque command vector $\mathbf{\Gamma}$ of size n and velocity command vector $\delta \mathbf{q}$, also of size n are both generated from the position/force duality tabulated in Table 1 to describe the desired end-effector motion trajectory and contact forces.

Since the arm is in torque control and the base in velocity control, the appropriate command for each joint is then sent accordingly. For example, let's take a combined system where the base

makes up the first 3 joints, and the arm the last 6. From the resulting $n \times 1$ velocity command vector $d\mathbf{q}$, the first 3 elements are sent to the base. Similarly, the last six elements of the torque command vector $\mathbf{\Gamma}$ are sent to the arm (see Figure 1).

Figure 1. Torque vector from operational space formulation and velocity vector from velocity control, are both generated to satisfy the desired trajectory. The commands are sent to the corresponding joints.

A mobile manipulator has typically redundant joints with respect to the task. It is then necessary to control the behaviour of the manipulator posture. Many algorithms have been proposed in the past, such as those by Klein and Huang (1983), Hsu et al. (1988), Nakamura and Hanafusa (1987), Yoshikawa (1984) and Angeles et al. (1988).

In this application, potential functions were constructed to have minima at the desired manipulator redundant behaviour. The inverse $\bar{J}$ as in Equation 2 ensure the projection of the gradient descent of the potential function onto the null space of J will not interfere dynamically with the end-effector task. These potential functions are designed to have minima at the desired postures. The null space torque and null space joint velocity are obtained by taking the gradient descent of the potential function.

$$\begin{aligned} \mathbf{\Gamma}_0 &= -\nabla V(\mathbf{q}), \text{ and} \\ \delta\mathbf{q}_0 &= -\nabla V(\mathbf{q}) \end{aligned} \tag{5}$$

where $\mathbf{\Gamma}_0$ and $\delta\mathbf{q}_0$ are the null space torque and joint velocity vectors as in the equations in Table 1.

The general expression for the potential function could be:

$$V(\mathbf{q}_i) = \frac{1}{2}\sum_i k_i[f(\mathbf{q}_i) - f(\mathbf{q}_{i(desired)})]^2 \tag{6}$$

5 Application to Aircraft Canopy Polishing

The proposed method was implemented on a torque-controlled PUMA 560 manipulator arm and a velocity-controlled Nomad XR4000 mobile base, as shown in Figure 1.

In this implementation, the holonomic Nomad XR4000 base is modelled as having 3 (planar) DOFs, namely translation along X and Y and rotation around Z axes. This is done because the control to the mobile base is available in high level control (velocity control). The Nomad actually has 4 wheel modules, with 2 actuators each, one for driving and one for steering.

The overall system is therefore thought of as a 9 jointed mechanism, with the base providing the first three velocity-controlled joints (two prismatic and one revolute), and the arm the last six torque-controlled joints (see Figure 2).

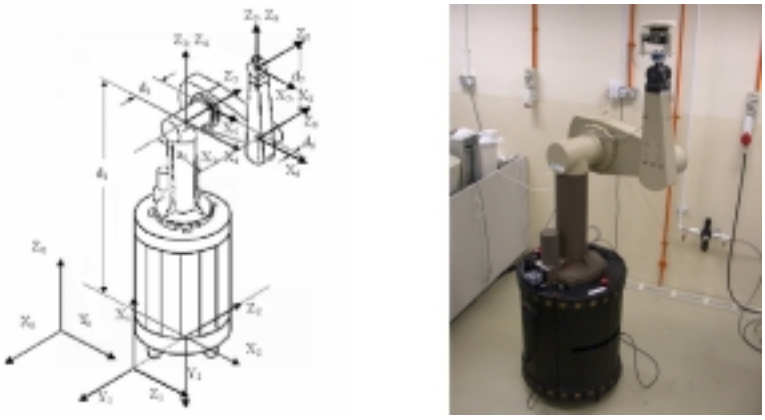

Figure 2. FRAME ASSIGNMENT FOR THE INTEGRATED SYSTEM

From this point onward, joint 1,2, and 3 would refer to the first three joints of the overall system, supplied by the base, and joint 4 to 9 would refer to joint 1 to 6 of the PUMA arm respectively.

The resulting Jacobian is of size 6 by 9. A 9 by 1 joint torque command and joint velocity command are generated by the equations summarized in Table 1. The first three elements of the velocity vector are sent are joint command to the mobile base, while the last 6 elements of the torque vector to the PUMA arm.

In dynamic compensation, the full dynamic model is employed for the PUMA arm, while only a simplified model is used for the Nomad base. The inertia matrix A used for the Nomad base is only modelled as having diagonal terms.

A PD control law is used for the motion control such that:

$$\mathbf{F}^*_{motion} = \mathbf{I}\ddot{\mathbf{x}}_d - \mathbf{k}_{v(motion)}(\dot{\mathbf{x}} - \dot{\mathbf{x}}_d) - \mathbf{k}_{p(motion)}(\mathbf{x} - \mathbf{x}_d) \tag{7}$$

and PI control for force control:

$$\mathbf{F}^*_{force} = -\mathbf{k}_{p(force)}(\mathbf{F}_{contact} - \mathbf{F}_d) - \mathbf{k}_{i(force)} \int (\mathbf{F}_{contact} - \mathbf{F}_d)dt \tag{8}$$

K_p and K_v gains were chosen to result in a slightly underdamped closed loop system with natural frequency $\omega_n = 45 rad/s$.

Force readings were taken with a JR3 FT sensors, with a low pass filter. PUMA and the NOMAD base were controlled by separate computers, linked by a high speed TCP/IP connection. Control calculation is done on the processor controlling PUMA and the velocity command vector $\delta\mathbf{q}$ is sent over to the NOMAD controller as high level velocity command.

Three sets of experimental result is shown in this paper, which analyze the performance of the combined arm-base system in free motion, constrained motion, and in an industrial application involving a canopy polishing task (see Figure 3).

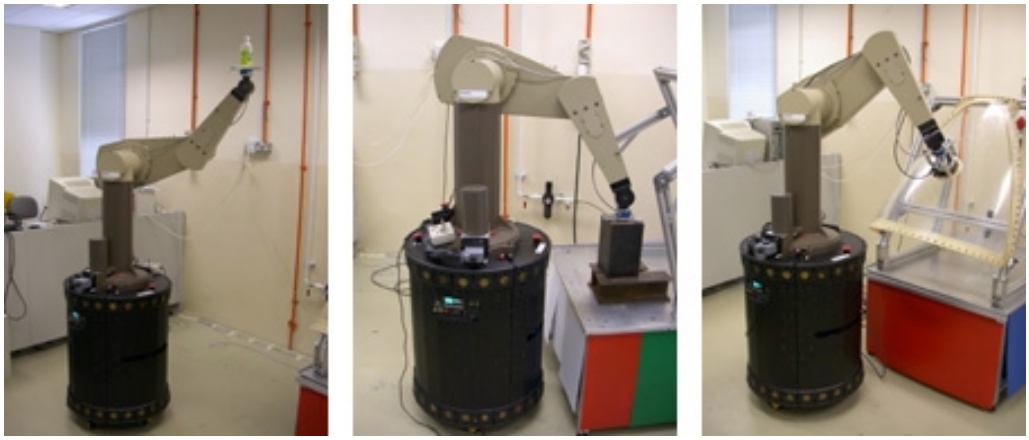

Figure 3. The three experiment setups: (left) maintaining stationary end-effector while the base moves in an elliptical trajectory (center) maintaining a normal force (stationary end-effector) with a moving base, and (right) polishing task, maintaining constant 10 N force normal to unknown surface with sinusoidal end-effector motion, with moving base.

5.1 Free motion

This task requires the mobile base to move in an elliptical trajectory, while maintaining the end-effector stationary with respect to the world frame. The error in motion tracking is shown as the result. Motion of the base while maintaining a stationary end-effector can be thought of as internal joint motion of the arm-base system. This motion is created by projecting the motion of the base into the null space of the Jacobian. The desired null space configuration $q_{i(desired)}$ for joint 1 and 2 (the translational DOF of the base) as in Equation 6 is made to follow a trajectory.

The error in motion trajectory tracking is shown in Figure 4. The result presents the motion tracking performance of the arm-base system. It is required to keep the end-effector stationary while the base moves in an ellipse, major axis 40 cm and minor axis 14 cm. The low speed setting was for the mobile base to complete the ellipse in 30s, and high speed in 10s, as shown in the lower graphs of Figure 4.

This graph shows that while velocity control of the base has been theoretically compensated for the dynamics of the structure, it is still affected by the disturbance of the base motion at high

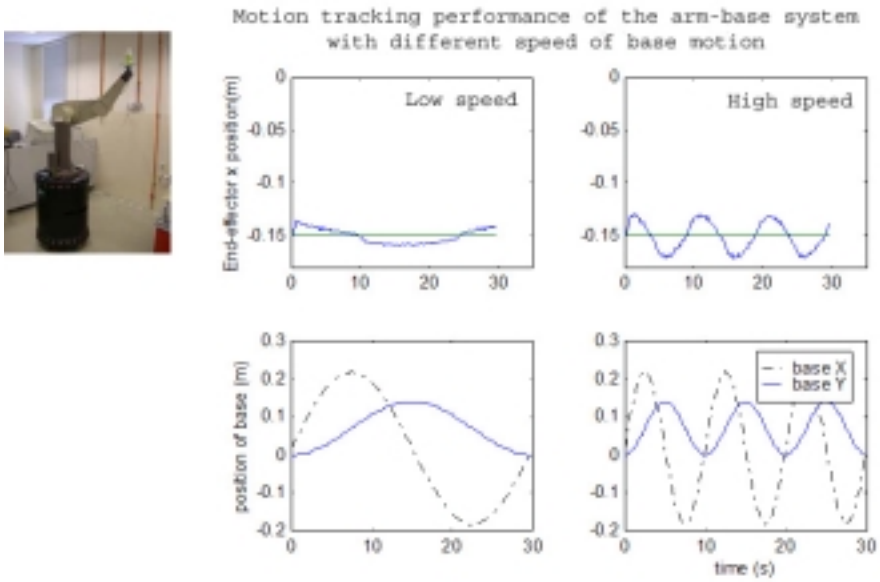

Figure 4. The motion tracking performance of the arm-base system. The mobile base was required to move in an elliptical trajectory of 40cm major axis and 14cm minor axis. The desired X position is -15cm. Tracking is shown with the mobile base moving in low speed (left) and high speed (right)

speed. In addition to the fact that the servo loop for velocity control is much slower than the internal servo loop, torque control is still necessary for high speed dynamic compensation.

The result only shows the tracking performance in X axis because the elliptical trajectory of the base motion has the major axis along X, and error is most prominent in this axis. Z axis has very little error because it is decoupled from the motion of the base.

The result in Figure 4 shows that the error is contained within $\pm$ 1 cm when the base moves in low speed and barely within 2 cm at high speed.

5.2 Constrained motion

This experiment compares the result of the force control ability of the system while the base is stationary and while the base is moving. The task was to track a desired force trajectory (against a surface) that switches between 20N and 15 N every 2 seconds while maintaining the end-effector position. Just like in Section 5.1, the motion of the base is created by projection to the null space of the Jacobian.

Figure 5 shows the performance of force control with a stationary base (left) compared to that with moving base (right). The error in force control at moving base is shown to be within $\pm$2.5N. The effect of dynamic disturbance of the mobile base of the performance of the arm is further discussed in Holmberg and Khatib (2000).

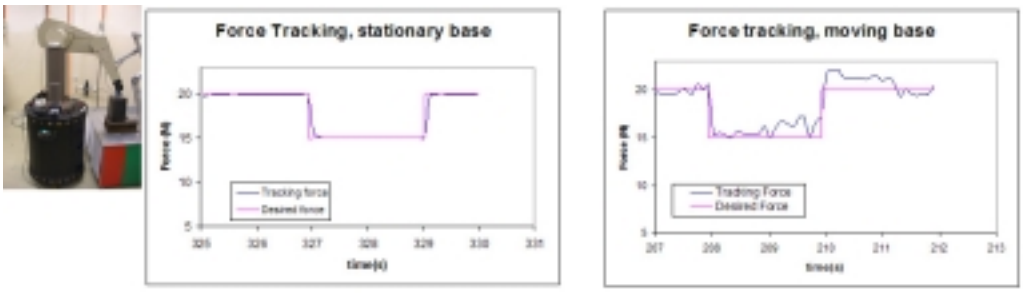

Figure 5. The system was required to perform force control by exerting a normal downward force to track the desired force trajectory. (left) force tracking performance of a stand alone (stationary) PUMA arm and (right) that of arm-base system with moving base.

5.3 Canopy polishing

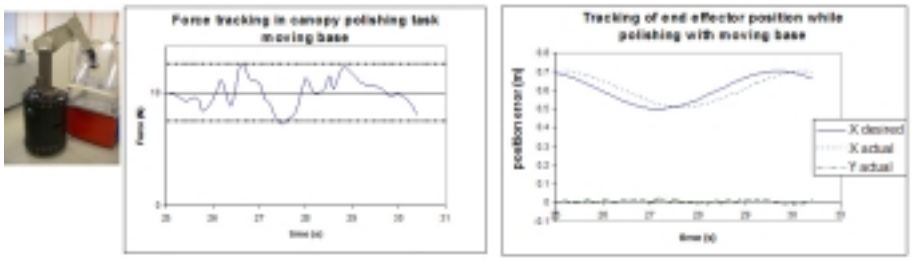

Figure 6. The system is required to perform sinusoidal tool motion maintaining 10N force normal to the unknown surface. The graph shows the error response of the mobile manipulator in force (right)) and position (right) tracking with moving and stationary base

This task requires the system to maintain a normal force of 10N against an unknown surface, while the end-effector moves in a sinusoidal manner. The mobile manipulator automatically complies to the unknown canopy geometry while trying to maintain a constant force of 10 N normal to the canopy surface. The result compares the performance of the system with a stationary and with a moving base.

The operational point is chosen at the end of the polishing tool. Motion control is applied to the translation along X and Y axes of the base frame, and the rotational around the Z axis of the tool frame. The 10N force exerted normal to the unknown canopy surface is along the Z axis of the tool frame. Moment control is applied to the other two remaining DOFs, namely rotation around X and Y of the tool frame. Maintaining the moments around these two axes at zero create the compliant motion of the polishing tool to follow the contour of the polished surface.

In this experimental run, internal joint motion was set so that the mobile base always faces the end-effector. This is to prevent the PUMA arm from hitting the limit of its first joint and to increase the system manipulability [Yoshikawa (1985)].

The potential function used was defined as:

$$V(\mathbf{q}) = k_d(q_4 - q_{4-desired})^2; \tag{9}$$

where $q_{4-desired} = 0$. This means we would like to keep joint 4 (first joint of PUMA arm) to be at the center of its range. The projection of the gradient descent of this potential function (Equation 5) onto the null space would cause the base to move accordingly.

The performance of the system with combined arm and base was found to be almost the same for stationary and moving base, therefore the graph in Figure 6 only shows the performance of the system with moving base. The force distribution (with the desired value being 10N) has a spread of ± 2 N in both cases, and motion tracking error within 7 cm.

When the tool moves sinusoidally while maintaining contact with the surface of the canopy, disturbance introduced by the friction with the surface seemed to overwhelm the error introduced by the dynamic disturbance of the base motion. In the paper by Jamisola et al. (2002), it was found that friction between the polishing tool and the surface contributed to much of this error. A friction compensation was implemented in the above mentioned experiment to reduce the effect.

The force control performance of maintaining the 10N contact force normal to the canopy surface within $\pm$ 2N was sufficiently accurate for the task.

The polishing motion can be seen from the video in
http://guppy.mpe.nus.edu.sg/ mpeangh/robotics/polishing-base.mpg.

6 Conclusion

The paper presented the method of using a velocity-controlled robot to be combined with a torque-controlled robot in performing a mobile manipulation task. The method was shown to be effective in performing a force and motion control task, while taking into account the dynamics of the robots. While ideally a torque-controlled base is required, the compensation by the lighter, faster, and more accurate arm was sufficient to cover the inaccuracy of the base for less demanding tasks. It is shown in the result that with fast motion of the base, the disturbance would start to affect the performance of the system noticeably. The method was implemented on a practical application of a canopy polishing task, which required a constant polishing force to be maintained and some additional workspace for the robot to cover the entire workpiece.

7 Acknowledgement

The work published in this paper is a part of the collaboration project between Gintic Institute of Manufacturing Technology, National University of Singapore, and Stanford University. The authors would like to thank Gintic and the members of the project team, especially to Dr Lim Ser Yong for his support and to Tao Ming Lim for the development of the programming platform.

References

Angeles, J., Habib, M., and L*ó*pez-Caj*ú*n, C. (1988). Efficient algorithms for the kinematic inversion of redundant robot manipulators. *The International Journal of Robotics and Automation* 3(1):106–116.

Chang, K., and Khatib, O. (1995). Manipulator control at kinematic singularities: A dynamically consistent strategy. *Proc. IEEE/RSJ Int. Conference on Intelligent Robots and Systems* 3:84–88.

Grabits, G. A. (1986). Polishing aerospace transparencies. *Conference on Robotic Solutions in Aerospace Manufacturing* MS86–203 1–22. Orlando, Florida.

Holmberg, R., and Khatib, O. (2000). Development and control of a holonomic mobile robot for mobile manipulation tasks. *International Journal of Robotics Research* 19(11):1066–1074.

Hsu, P., Hauser, J., and Sastry, S. (1988). Dynamic control of redundant manipulators. *IEEE Intl. Conf. Robotics and Automation* 1:183–187.

Jamisola, R., Lim, T. M., Oetomo, D., Ang, M., Khatib, O., and Lim, S. Y. (2002). The operational space formulation implementation to aircraft canopy polishing using a mobile manipulator. *Accepted to the Proc. of Intl. Conf. Robotics and Automation, May 2002*.

Khatib, O., Yokoi, K., Brock, O., Chang, K., and A.Casal. (1999). Robots in human environments: Basic autonomous capabilities. *The International Journal of Robotics Research* 18(7):684–696.

Khatib, O. (1987). A unified approach for motion and force control of robot manipulators: The operational space formulation. *IEEE J. Robotics and Automation* RA-3(1):43–53.

Klein, C., and Huang, C. (1983). Review of pseudoinverse control for use with kinematically redundant manipulators. *IEEE Trans. Sys., Man., Cyber.* SMC-13(3):245–250.

Nakamura, Y., and Hanafusa, H. (1987). Optimal redundancy control of robot manipulators. *International Journal of Robotics Research* 6(1):32–42.

Whitney, D. (1969). Resolved motion rate control of manipulators and human prostheses. *IEEE Trans. Man-Machine Sys.* MMS-10(2):47–53.

Yoshikawa, T. (1984). Analysis and control of robot manipulators with redundancy. In Brady, M., and Paul, R., eds., *Robotics Research*. Cambridge, MA: MIT Press. 735–747.

Yoshikawa, T. (1985). Manipulability of robotic mechanisms. *Intl. J. Robotics Research* 4(2):3–9.